

# Chemistry A European Journal





# **Accepted Article**

**Title:** On the Reactivity Enhancement of Graphene by Metallic Substrates towards Aryl Nitrene Cycloadditions

Authors: Xiaojian Yang, Feiran Chen, Min A Kim, Haitao Liu, Lawrence M Wolf, and Mingdi Yan

This manuscript has been accepted after peer review and appears as an Accepted Article online prior to editing, proofing, and formal publication of the final Version of Record (VoR). This work is currently citable by using the Digital Object Identifier (DOI) given below. The VoR will be published online in Early View as soon as possible and may be different to this Accepted Article as a result of editing. Readers should obtain the VoR from the journal website shown below when it is published to ensure accuracy of information. The authors are responsible for the content of this Accepted Article.

To be cited as: Chem. Eur. J. 10.1002/chem.202100227

Link to VoR: https://doi.org/10.1002/chem.202100227

#### **FULL PAPER**

# On the Reactivity Enhancement of Graphene by Metallic Substrates towards Aryl Nitrene Cycloadditions

Xiaojian Yang, [a],# Feiran Chen, [a],# Min A Kim, [b] Haitao Liu [b],\*, Lawrence M. Wolf [a],\*, Mingdi Yan [a],\*

 [a] Dr. X. Yang, F. Chen, Prof. L. M. Wolf. Prof. M. Yan Chemistry Department University of Massachusetts Lowell One University Ave, Lowell, MA 01854 (USA) E-mail: Lawrence\_Wolf@uml.edu, Mingdi\_Yan@uml.edu

[b] M. A. Kim, Prof. H. Liu
 Department of Chemistry
 University of Pittsburgh
 219 Parkman Ave., Pittsburgh, PA 15260 (USA)
 E-mail: hliu@pitt.edu

These authors contributed equally to this work.

Supporting information for this article is given via a link at the end of the document.

Abstract: Pristine graphene is fairly inert chemically, and as such, most application-driven studies use graphene oxide, or reduced graphene oxide. Using substrates to modulate the reactivity of graphene represents a unique strategy in the covalent functionalization of this otherwise fairly inert material. We found that the reactivity of pristine graphene towards perfluorophenyl azide (PFPA) can be enhanced by a metal substrate on which graphene is supported. Results on the extent of functionalization, defect density, and reaction kinetics all show that graphene supported on Ni (G/Ni) has the highest reactivity toward PFPA, followed by G/Cu and then G/silicon wafer. DFT calculations suggest that the metal substrate stabilizes the physisorbed nitrene through enhanced electron transfer to the singlet nitrene from the graphene surface assisted by the electron rich metal substrate. The G/Ni substantially stabilizes the singlet nitrene relative to G/Cu and the free-standing graphene. The product structure is also predicted to be substrate dependent. These findings open up opportunities to enhance the reactivity of pristine graphene simply through the selection of the substrate. This also represents a new and powerful approach to increasing the reactivity of singlet nitrenes through direct electronic communication with graphene.

#### Introduction

Graphene has demonstrated a wide range of exceptional thermal, mechanical and electronic properties, and holds great potential to revolutionize a number of technologically important areas including materials science, microelectronics, and biomedical science. The potential, however, has been hampered by the poor processability of pristine graphene due to its limited solubility. In this context, the ability to functionalize pristine graphene enables the introduction of well-defined chemical functionalities, modulate the product solubility, open the otherwise zero-gap electronic band of pristine graphene, and enable its integration into high performance composite materials and devices. [2,3]

Pristine graphene contains exclusively conjugated  $sp^2$  carbons, having its  $\pi$  electrons delocalized over the entire 2D network. The large resonance stabilization makes it fairly inert

chemically, which poses considerable challenges to the chemical functionalization of pristine graphene. Thus, the covalent chemistry on pristine graphene has traditionally required highly reactive species such as free radicals, carbenes and nitrenes.[4] A grand challenge in graphene chemistry would be to expand the chemical space and enable a wide range of reactions on pristine graphene. As such, methods for enhancing the reactivity of pristine graphene are especially attractive. Like many nanoscale materials, the dangling bonds on the graphitic edges of graphene make the edges more reactive than the basal plane. Thus, one way to increase the reactivity of pristine graphene is to increase the number of edges and defect sites on graphene. Different methods, including lithography, have been used to intentionally create defects and holes in the graphene basal plane to make the so-called holey graphene or graphene nanomeshes.[5] However, these physical defects damage the integrity of the graphene material, limiting their wide adoptions.

Enhanced reactivity has been reported for graphene under mechanical strains or deposited on substrates that can induce large charge fluctuations. In these cases, high quality pristine graphene was used, and the structure of the starting material was preserved. For example, Ruoff and coworkers deposited monolayer graphene on silicon wafer covered with silica nanoparticles, and observed that the reaction with aryl radicals occurred only in the regions of graphene situated on top of the nanoparticles.<sup>[6]</sup> This was attributed to the local mechanical strain imposed on graphene by the nanoparticles underneath, which led to enhanced reactivity of the pi bonds, similar to carbon nanotubes and fullerenes. In the reaction with a diazonium salt, Strano and coworkers reported higher product yields for graphene supported on surfaces of SiO<sub>2</sub> and Al<sub>2</sub>O<sub>3</sub> than those having less charge fluctuations like alkyl-terminated SiO2 and hexagonal boron nitride (hBN).[7]

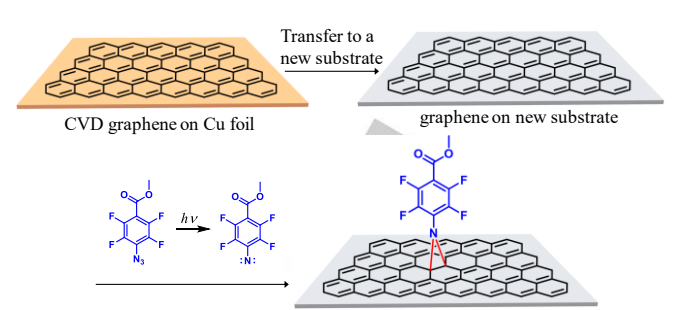
We have developed an efficient chemistry to covalently functionalize pristine graphene using perfluorophenyl azide (PFPA). [8] Activation of PFPA by heat, microwave, or UV leads to the generation of the highly reactive singlet perfluorophenyl nitrene, which undergoes C=C addition reaction with graphene. [9] The reaction can be used to render graphene soluble in either

#### **FULL PAPER**

organic solvents or water,<sup>[10]</sup> to create lithographically patterned structures,<sup>[11]</sup> and to conjugate nanoparticles.<sup>[12]</sup> In this work, we investigate the impact of the substrate on the reactivity of graphene with PFPA. As the reaction proceeds through the highly electron-deficient singlet perfluorophenyl nitrene, we hypothesize that the reactivity can be modulated by the charge density on graphene. This will be achieved by adsorption of graphene on a metal substrate.

Two different metals were used in the study: Ni and Cu. The graphene-metal interface has been extensively studied, concluding that the adsorption of graphene on a substrate can substantially change the electronic properties of graphene, including the charge density, binding energy and distance between graphene and the substrate. [13] Two types of interactions have been suggested based on the binding energy and equilibrium separation distance: (1) chemisorption in the cases of Co. Ni. Pd (111) and Ti (0001), and (2) physisorption in the cases of Al, Cu, Ag, Au and Pt (111).[14] Ni is a strongly interacting metal with graphene, giving a short equilibrium separation of  $2.11 \pm 0.07$ Å between graphene and Ni. far less than other metals like Cu (3.26 Å) or Au (3.31 Å).[15] Consequently, both the physical and chemical properties of graphene are significantly altered, including band gap opening by 2 eV below the Fermi-level and the lengthening of the carbon-carbon bond. [13b] The orbital hybridization also leads to charge redistribution, implying electron accumulation close to the graphene surface. [16] Despite extensive computational work, experimental study remains limited, and the underlying mechanism of how Ni as the substrate impacts the reactivity of graphene is still unclear. In one example, the reactivity of CO on graphene supported on Ni(111) was studied, showing CO chemisorbed on graphene grown on Ni(111) with much higher adsorption energy (0.35-0.58 eV) than CO physisorbed on free-standing graphene (~0.1 eV).[17] DFT calculations showed that chemisorption of CO graphene/Ni(111) led to the formation of an ethylene dione complex (C2O2), which co-adsorbed with O2 and subsequently produced two molecules of CO<sub>2</sub>.<sup>[17d]</sup>

In this work, we carried out the reaction between PFPA and graphene supported on Ni or Cu. Silicon wafer (SiO2/Si) was chosen as a control substrate. Although electron-hole fluctuation has also been observed in SiO2, [7] the impact to the charge density of graphene is expected to be substantially less than metals. Single-layer graphene fabricated by chemical vapor deposition (CVD) was first transferred to Ni, Cu or silicon wafer, and was then allowed to react with PFPA by photoactivation (Scheme 1). The products were analyzed by Raman spectroscopy and mapping. The computational investigation into the origins of the substrate effect using DFT revealed that increased charge transfer to the perfluorophenyl nitrene intermediate was responsible for the activity enhancement. The substrate is also shown to significantly influence the singlet-triplet gap of the nitrene, further stabilizing the active singlet perfluorophenyl nitrene. The results of this work suggest that substrate activation represents an effective and novel strategy for functionalizing graphene using nitrenes, which may extend to other electron deficient reactants.



**Scheme 1.** Reaction of PFPA with graphene supported on a substrate. CVD graphene fabricated on a Cu foil was first transferred to the new substrate by a poly(methyl methacrylate) (PMMA)-assisted transfer process. Photochemical activation of PFPA led to the formation of the singlet perfluorophenyl nitrene which subsequently reacted with graphene to form the covalent adduct.

#### **Results and Discussion**

Fabrication of graphene in Ni and Cu film. Graphene was fabricated by CVD, as the method produced reasonably high quality of single-layer graphene with accessible equipment. All graphene starting materials were prepared on Cu foils on a homebuilt apparatus to minimize defects and contamination. Prior to graphene deposition, the Cu foils were subjected to a brief electropolishing treatment to clean the surface and to reduce the surface roughness. Graphene was obtained by annealing the Cu foil in the tube furnace at 1000 °C under H2 for 30 min, followed by CH<sub>4</sub> for 30 min. The vast majority of the CVD graphene prepared on the Cu foil consisted of monolayer graphene, shown in the Raman spectra which contained the characteristic narrow G band and symmetrical 2D band (Figure S1A). The defects, judged by the peak intensity of the D band which requires the existence of defects to activate, was low. The intensity ratio of the D vs. G band,  $I_D/I_G$ , was 0.059 ± 0.020, measured from ~300 data points on CVD graphene samples from different batches (Figure.

Ni and Cu substrates were prepared by depositing 100 nm thick Ni or Cu film on silicon wafer using an electron-beam (EB) evaporator. CVD graphene fabricated on Cu foil was transferred to Ni, Cu or SiO<sub>2</sub>/Si following the poly(methyl methacrylate) (PMMA)-assisted transfer process.[18] Briefly, a PMMA layer was spin-coated on graphene, and the Cu foil was etched away in FeCl<sub>3</sub>/HCl. The PMMA-backed graphene was then placed on the new substrate, and the PMMA layer was removed with acetone to give graphene supported on Ni, Cu or SiO<sub>2</sub>/Si (G/Ni, G/Cu, G/SiO<sub>2</sub>/Si). G/SiO<sub>2</sub>/Si showed intense Raman signals (black curve, Figure 1A). The signal enhancement is known to be the result of the trilayer construct - consisting of the sample (graphene), capping layer (SiO<sub>2</sub>) and substrate (Si) - which provides multiple pathways for interference between all transmitted light in the graphene sheet as well as multiple reflections of scattering Raman light in graphene at the graphene/air and graphene/SiO<sub>2</sub> interfaces.<sup>[19]</sup> At 532 nm incident laser power and 300 nm SiO<sub>2</sub> layer thickness, the signal enhancement can be over 10 times, thus giving Raman absorption bands having high signal intensities.[19]

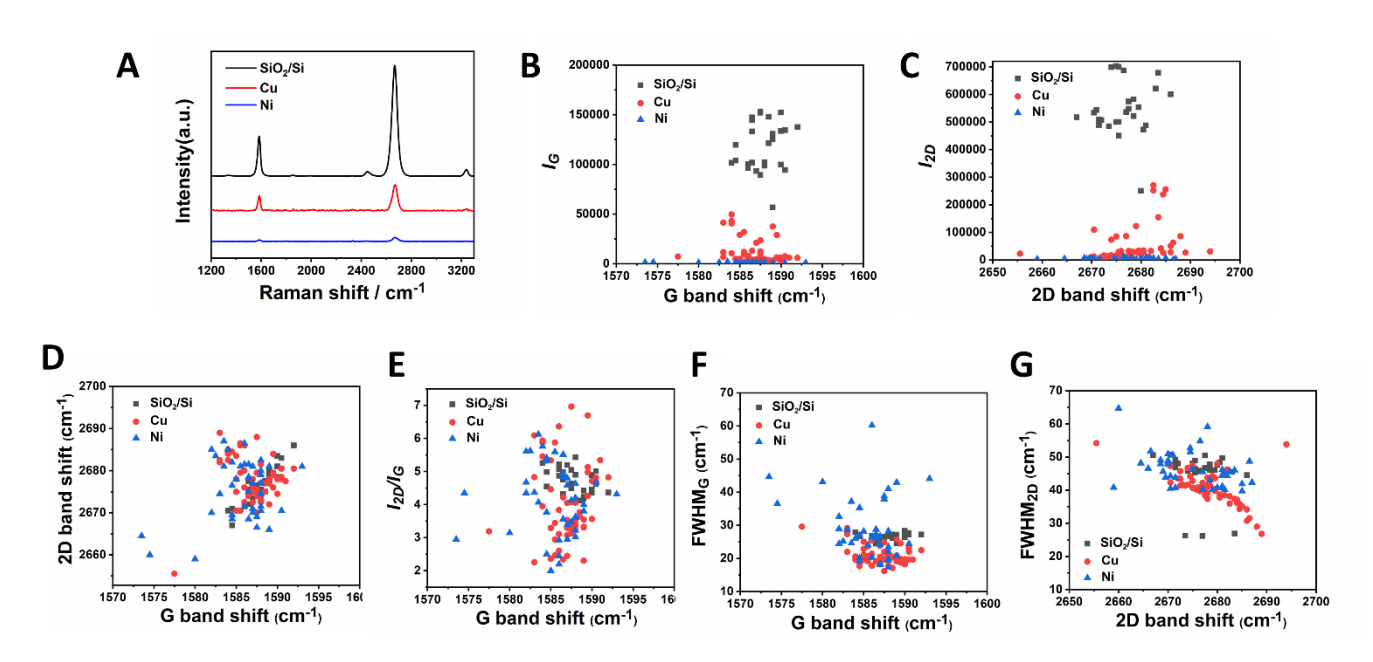


Figure 1. (A) Representative Raman spectra of G/Ni (blue), G/Cu (red), or G/SiO<sub>2</sub>/Si (black). The spectrum of G/Cu was background corrected. (B) and (C) are the intensity of G band or 2D band vs. band position, respectively. (D) 2D band position vs. G band position. (E)  $I_{2D}/I_G$  vs. G band position. (F) FWHM of G band vs. G band position. (G) FWHM of 2D band vs. 2D band position. Data were collected on a Bruker SENTERRA II Raman microscope having a spectral resolution of 0.5 cm<sup>-1</sup>, using a 532 nm laser (2.33 eV).

For G/Ni and G/Cu, the intensities of the Raman G band and 2D band were greatly diminished (red and blue curves, Figure 1A). The decrease was the largest for G/Ni. The suppression of graphene Raman signals by Ni is well-known, attributed to the strong interaction between Ni and graphene originated from the 3d-p orbital hybridization, giving rise to a large difference in the pz band energy and the loss of the phonon-photon resonance in graphene.<sup>[20]</sup> For graphene chemisorbed on Ni(111), the strong interaction can lead to the complete disappearance of the Raman signals. [20a] For metal substrates where the distance between graphene and the substrate is larger than that of graphene-Ni, the orbital hybridization is less pronounced, thus the graphene-metal interactions are much weaker. On Cu, graphene is only physisorbed by van der Waals forces with a large Cu-graphene separation at 3.3 Å.[15a] As such, the impact from the substrate is weaker and Raman spectra are possible to collect for graphene supported on these metals. On the other hand, the interfaceinduced Raman enhancement effect observed in the case of SiO<sub>2</sub>/Si is absent for Cu, and therefore the signal intensities are weaker for graphene supported on Cu.[21] Furthermore, the Raman spectrum of G/Cu contains a broad background peak that is from the photoluminescence of the Cu substrate (Figure S2), which needs to be background corrected (cf. red curve, Figure

Figures 1B and 1C plot the intensity of G band ( $I_G$ ) or 2D band ( $I_{2D}$ ) of G/Ni, G/Cu and G/SiO<sub>2</sub>/Si. Here, the intensity was the integrated area under each peak instead of the peak height, as the peak area includes all possible Raman scattering and thus the data would be more accurate especially for samples with small D bands. [22] It is clear that both  $I_G$  and  $I_{2D}$  were the highest for G/SiO<sub>2</sub>/Si, much lower for G/Cu and very weak for G/Ni. Although

the d-p orbital hybridization can drastically decrease the Raman signal intensity, for example, no D or 2D bands were seen for graphene on lattice matched Ni(111),<sup>[20b]</sup> Raman spectra have nevertheless been recorded for graphene on Ni. Kim et al. reported the Raman spectrum of single-layer graphene fabricated on EB-evaporated Ni film (300 nm) that contained weak but characteristic G (~1580 cm<sup>-1</sup>) and 2D (2689 cm<sup>-1</sup>) bands.<sup>[23]</sup> The data in Figure 1 indicated that the CVD graphene transferred to the EB-evaporated Ni film was physisorbed rather than chemisorbed. The significantly weakened signal intensities imply that the electronic property of graphene on Ni was much more impacted than that on Cu.

Figures 1D–1G are the plots of 2D band vs. G band position (Figure 1D),  $I_{2D}/I_G$  vs. G band position (Figure 1E), FWHM (full width at half maximum) of G band vs. G band position (Figure 1F). and FWHM of 2D band vs. 2D band position (Figure 1G). Since the signal intensities were significantly lower on the metal substrate (Figures 1B, 1C) than on SiO<sub>2</sub>/Si, the data for G/Ni and G/Cu were much more scattered. This was especially true for G/Ni as the intensities of the Raman signals were barely above the background noise, thus creating large variations of the values. Nevertheless, several observations can be made from the data of G/SiO<sub>2</sub>/Si. (1) The positions of G band (1584-1592 cm<sup>-1</sup>) and 2D band (2665-2688 cm<sup>-1</sup>) were within the range of what are expected for pristine single-layer graphene. (2) The  $I_{\rm 2D}/I_{\rm G}$  was in the range of 4-5.5. (3) The FWHM was fairly narrow for G band (25-28 cm<sup>-1</sup>), wider for 2D band (25-50 cm<sup>-1</sup>) although most were in the range of 45-50 cm<sup>-1</sup>.

In this work, the intensity ratio of Raman D and G peaks  $(I_D/I_G)$  is used to quantify the extent of functionalization on graphene. This practice has adopted wide use, made possible as

 $I_{\rm G}$  is proportional to the number of sp<sup>2</sup> C atoms in graphene and remains constant at low levels of defects (distance between point defects  $L_{\rm D}$  > ~10 nm). [22,24] The Raman D band, which is absent in intensity due to physical defects, Raman spectra were collected on areas of the samples without visible defects.

To investigate whether the transfer process would introduce physical defects to the sample, CVD graphene fabricated on the Cu foil was first transferred to the Cu film, then to silicon wafer. The Raman spectrum of this twice-transferred graphene (red curve, Figure S3) was similar to that of graphene transferred only once from Cu foil directly to silicon wafer (black curve, Figure S3), without any detectable increase in the D peak intensity. This demonstrates that the additional transfer step in the cases of Ni and Cu did not lead to an increase in the D band intensity.

#### Reaction of substrate-supported graphene with PFPA

Methyl 4-azido-2,3,5,6-tetrafluorophenylbenzoate (PFPA, Scheme 1), synthesized following a previously reported procedure, was used as the model compound in this study. [12] We have conducted extensive studies on the reaction of PFPA with graphene, including detailed analysis of the covalent product by XPS.[8-11,12b,26] In this study, we focus on the effect of metal substrate on the reactivity of PFPA. The reaction was carried out by immersing the sample in a solution of PFPA in N-methyl-2pyrrolidone (NMP) and irradiating with a medium pressure Hg lamp in the presence of a 280-nm long-pass filter (intensity: 2.6 mJ/cm<sup>2</sup> at 365 nm). For G/Ni and G/Cu, the reacted graphene was further transferred to silicon wafer for the subsequent Raman analysis. Figure 2 are the Raman spectra of G/Ni before and after reaction with PFPA. The characteristic D peak at 1350 cm<sup>-1</sup> appeared in the product after 15 min irradiation, and the intensity increased with the irradiation time.

It has been reported that polyaromatic compounds like naphthalene, anthracene and pyrene could adsorb on the graphene surface through  $\pi\text{-}\pi$  stacking interactions.  $^{[27,28]}$  To rule out the possibility that the change in the Raman spectrum was due to the physisorption of PFPA molecules on the graphene surface, a control experiment was carried out where G/Ni was treated with methyl pentafluorophenylbenzoate (PFB), an analogue of PFPA except that the azide was replaced with F, under the same condition as in the case of PFPA. Compared to the samples treated with PFPA (Figure S4A), no obvious D peak or change in the Raman spectrum was observed in the case of PFB (Figure S4B), implying that the physical adsorption of pentafluorophenyl ring did not cause any changes in the Raman spectrum under the experimental conditions.

It has also been reported that monolayer CVD graphene could undergo oxidation under UV-ozone exposure, leading to spectral changes and increase in the D band intensity. [29] To investigate the impact of UV irradiation, G/Ni in the NMP solvent was subjected to the same reaction conditions, with the exclusion of PFPA. The Raman spectra of the resulting samples were similar to the untreated graphene (Figure S4C). No significant D peak was observed, in contrast to the spectra of graphene functionalized with PFPA (Figure S4A).

To confirm that the reaction with PFPA could occur on the basal plane of graphene, we carried out the reaction on mechanically-exfoliated HOPG, a material that consists of many layers of pristine graphene sheets held together by van der Waals forces and is widely accepted as the highest quality graphene material. HOPG was mechanically exfoliated onto silicon wafers using a Scotch tape. As the monolayer graphene on silicon wafers

defect-free graphene, becomes activated as a result of physical defects or when the sp<sup>2</sup> carbons are converted to sp<sup>3</sup> by chemical functionalization. To minimize the contribution of the D band fell off from the substrate after the reaction, multilayer graphite was used instead in this study. Multilayers are much easier to prepare in large pieces and high quality by the Scotch-tape method than the monolayer graphene, which is often much smaller in size, irregular and tends to have physical defects. As the top layer of HOPG graphite consists of high-quality pristine graphene, it will allow us to confirm that the reaction with PFPA could occur on the basal plane of graphene.

The Raman spectrum of the mechanically-exfoliated HOPG showed a broad and unsymmetrical 2D peak typical of multilayer graphene (black curve, Figure S5). The D peak was absent, confirming the high quality of the sample. The sample was then subjected to reaction with PFPA under the same condition as the CVD graphene. The Raman spectrum of the product contained a small D peak compared to the starting material (red curve. Figure S5). The intensity of the D peak is relatively low, as the reaction occurred only on the top layer and the bulk of the graphite was intact. Additionally, a D' peak at ~1615 cm-1 emerged (red curve and insert, Figure S5). The D' band in graphite originates from the intravalley phonon and is associated with scattering from the defects.[30] The FWHM of the G peak increased from 16.8 cm<sup>-1</sup> to 18.8 cm<sup>-1</sup>, a result that could be attributed to the disordered electronic environment within HOPG after the functionalization. The product was further characterized by FTIR, which showed absorptions corresponding to the PFPA (Figure S6). Taken together, these data demonstrate that the reaction could indeed occur on the basal plane of graphene.

The reactions were carried out using 0.1 M PFPA for 60 min, based on the studies on the optimization of reaction conditions (see Supplementary Information and Figure S7 for details). Figure 2A are the typical Raman spectra of graphene after the reaction with PFPA. The as-prepared CVD graphene had low initial defect, having  $I_D/I_G$  in the range of 0 – 0.1 (orange, Figure 2B). After reaction with PFPA,  $I_D/I_G$  increased for all graphene samples. A clear trend can be seen from the histograms of  $I_D/I_G$ , suggesting the influence of the substrate on the reactivity. The change in  $I_D/I_G$ was the highest in the case of G/Ni, followed by G/Cu, and  $G/SiO_2/Si$  was the least. Apart from the increase in  $I_D/I_G$ , the distribution also broadened after the reaction, implying spatial heterogeneity across the product surface. G/Ni showed the largest variation among all samples (0.1 - 0.53), of which the highest  $I_{\rm D}/I_{\rm G}$  value reached 0.53. This is followed by G/Cu in the range of 0.12 - 0.4, and  $G/SiO_2/Si$  in the range of 0.05 - 0.2.

Figure 2C plots the 2D band vs. G band position. Both the G band and the double resonance 2D band shifted to higher wavenumbers after functionalization. The upshift of G band and 2D band can be initiated by mechanical compression, doping or chemical functionalization. In our case, the change is attributed to chemical functionalization, as the graphene products were supported on silicon wafers so changes due to physical impacts would be similar for all samples. The increases in G and 2D wavenumbers for G/Ni and G/Cu were higher (orange shade) than G/SiO<sub>2</sub>/Si or unfunctionalized graphene (gray shade), indicating a higher extent of functionalization for G/Ni and G/Cu compared to G/SiO<sub>2</sub>/Si. In Figure 2D where  $I_{2D}/I_{G}$  was plotted against G band shift, G/Ni and G/Cu showed slightly lower (orange shade) values of 2.5 – 6 compared to 3.5 – 7 for G/SiO<sub>2</sub>/Si and pristine graphene (gray shade). This subtle difference also

reflects the difference in the extent of functionalization as well as the reactivity of graphene on different substrates, as higher functionalization is expected to result in more electron disordering and thus lower  $I_{\rm 2D}/I_{\rm G}$ . When plotting FWHM of G and 2D bands against their peak positions, there again showed two regions which separated G/Ni and G/Cu from that of G/SiO<sub>2</sub>/Si

and unfunctionalized graphene (Figures 2E, 2F). Although the changes were small, collectively, the results presented in Figures 2A–2F revealed a higher extent of functionalization of G/Ni and G/Cu than G/SiO<sub>2</sub>/Si, hinting an enhanced reactivity resulting from the metal substrate.

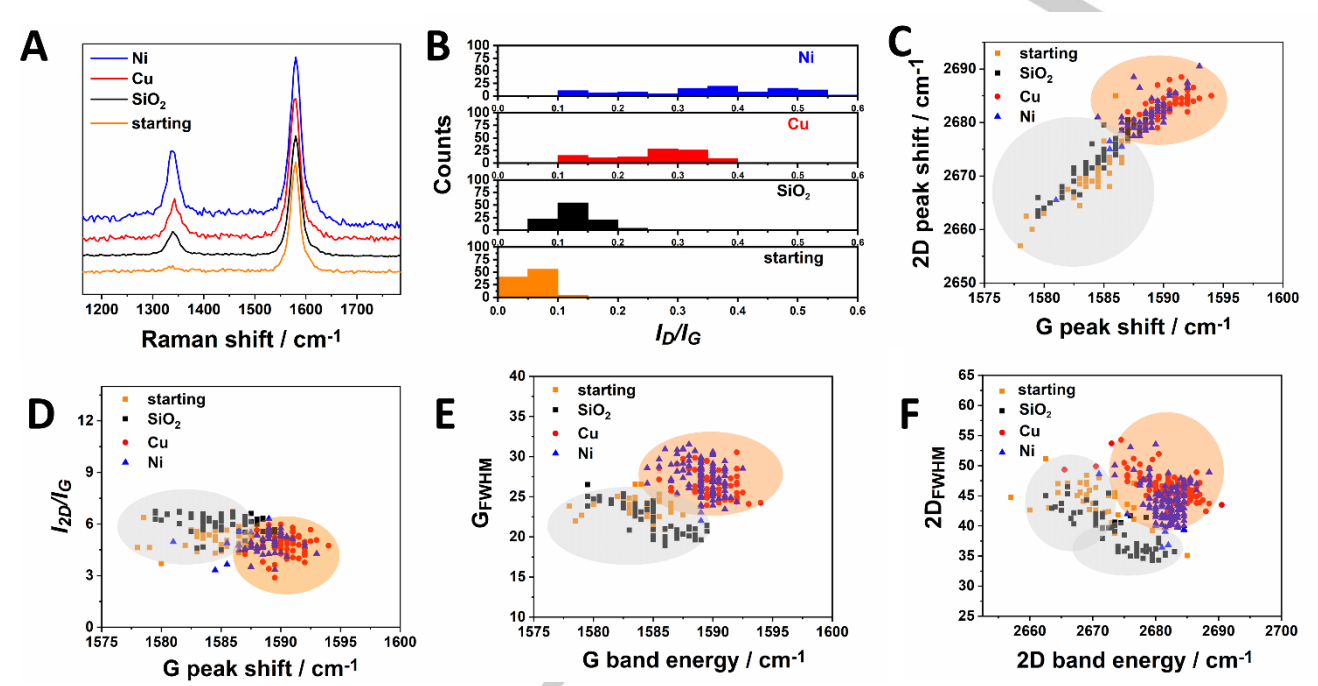


Figure 2. Raman characteristics of  $G/SiO_2/Si$  (orange), and after reaction with PFPA for  $G/SiO_2/Si$  (black), G/Cu (red) or G/Ni (blue): (A) representative Raman spectra (a.u.: arbitrary unit), (B) histograms of  $I_0/I_G$ , (C) 2D band vs. G band position, (D)  $I_2D/I_G$  vs. G band position, (E) FWHM of G band vs. G band position, and (F) FWHM of 2D band vs. 2D band position. All data were collected using 532 nm laser (2.33 eV). For G/Ni or G/Cu, the samples were transferred to silicon wafers prior to taking the spectra. The spectra in (A) and data in (B) were obtained on a Raman imaging microscope, with the spot size of 10  $\mu$ m×10  $\mu$ m. Data in (B) were calculated from 2 sets of independent samples. Data in (C)-(F) were collected on a Raman microscope, which has a resolution of 0.5 cm<sup>-1</sup>. About 50 spots on each sample were recorded.

To gain understanding on the extent of functionalization of graphene by PFPA, we employed a model that was developed to quantify the defects in graphene using Raman  $I_D/I_G$  values.<sup>[32]</sup> The model was built on experimental data from graphene functionalized by Ar+ ion bombardment,[22,32,33] and has been applied to other reaction systems including reduction reaction using a Na/K alloy[34] or lithium and biphenyl,[35] and Diels-Alder reaction. [36] Two parameters,  $L_D$ , the distance between the point defects, and the defect density  $n_{\rm D}$ , defined as the number of point defects per cm<sup>2</sup>, were used to describe the extent of functionalization. At low degree of functionalization ( $L_D > 3$  nm),  $L_{\rm D}$  decreases with increasing  $I_{\rm D}/I_{\rm G}$ , whereas at high degree of functionalization ( $L_D$  < 3 nm), the trend is reversed. By examining the Raman spectra of PFPA-functionalized samples, especially the peak widths of the G and the 2D bands as well as the absence of substantial D' and D+D' bands, [22,32,33] it was evident that  $L_D$  of our samples would be greater than 10 nm. We then computed  $L_D$ and  $n_D$  before and after the reaction with PFPA, shown in Figure 3 (see Supporting Information for detailed calculations, and the spatial mapping in Figure S8).

After reaction with PFPA,  $L_{\rm D}$  decreased to ~26 – 36 nm, ~19 – 25 nm and ~16 – 22 nm for the majority samples of G/SiO<sub>2</sub>/Si, G/Cu and G/Ni, respectively (Figure 3A). The data confirmed our assumption that the  $L_{\rm D}$  values of PFPA-functionalized graphene were greater than 10 nm. The defect density  $n_{\rm D}$  increased after the reaction, with the highest numbers observed for G/Ni, followed by G/Cu and then G/SiO<sub>2</sub>/Si. From the defect density  $n_{\rm D}$  and the reaction time course data in Figure 3B, assuming a pseudo-first order reaction kinetics under the experimental condition of [PFPA] >> [graphene], the pseudo-first order rate constants were estimated to be 3.8 × 10<sup>-2</sup> min<sup>-1</sup>, 1.7 × 10<sup>-2</sup> min<sup>-1</sup> and 1.0 × 10<sup>-2</sup> min<sup>-1</sup> for G/Ni, G/Cu and G/SiO<sub>2</sub>/Si, respectively (see Figure S9 and Supplementary Information for detailed calculations).

Taken together, the results consistently showed that the reactivity of graphene was affected by the nature of the substrate on which it was supported. The metal substrate enhanced the reactivity of graphene towards PFPA, and the enhancement followed the rank order of Ni > Cu >  $SiO_2/Si$ .

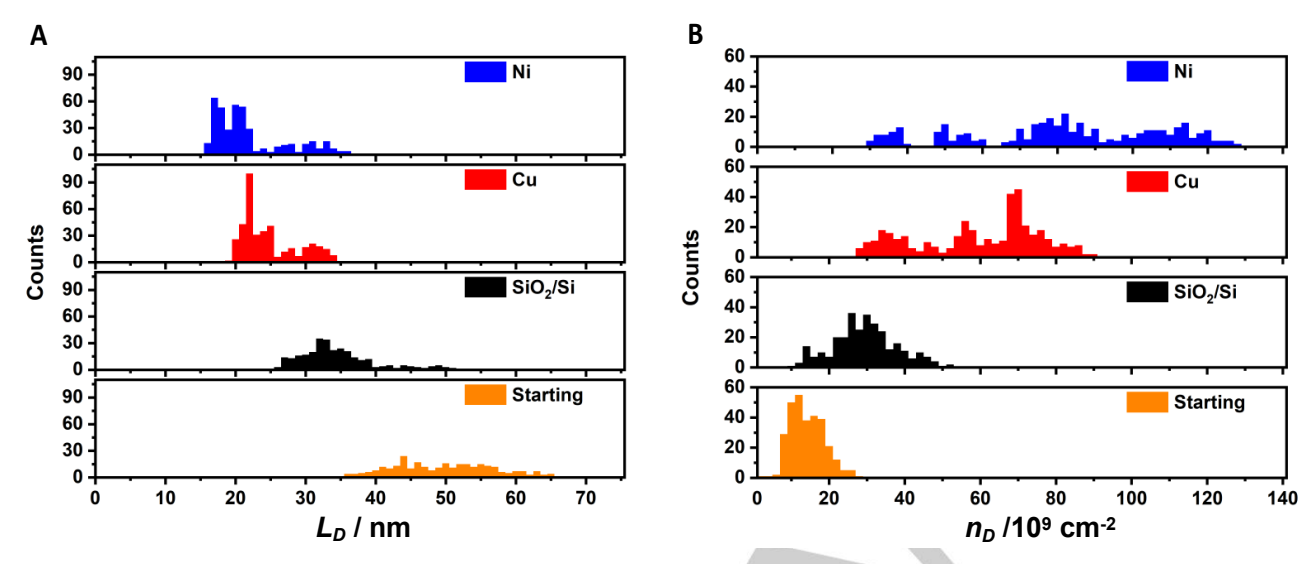


Figure 3. (A) The distance between the point defects,  $L_D$ , and (B) the defect density,  $n_D$ , of G/SiO<sub>2</sub>/Si (orange), and after reaction with PFPA for G/SiO<sub>2</sub>/Si (black), G/Cu (red) or G/Ni (blue).

In an effort to better understand the role of the substrate in enhancing the reactivity, DFT calculations were performed using the PBE<sup>[37]</sup> functional with the D2 dispersion correction<sup>[38]</sup> using ultra-soft pseudopotentials. The method was used to initially model a 6x6 graphene sheet adhered to Cu(111) and Ni(111) metallic substrates for initial validation against experimental and computationally determined results. The predicted interlayer separation distance between the graphene sheet and Cu(111) and Ni(111) surface was 3.09 Å and 2.14 Å respectively, which are reasonably close to the experimentally<sup>[15a]</sup> and prior computationally<sup>[39]</sup> determined values (Figure S10).

The reaction energy diagrams were next explored for the aziridination on graphene (G), and for graphene on Cu(111) (G/Cu) (Figure 4). The PFPA is first allowed to physisorb to the graphene surface to form **INT0** from the initial state, IS, at infinite separation. The PFPA physisorbs slightly more strongly to the

G/Cu by 2.6 kcal·mol<sup>-1</sup>. Upon photo-excitation, PFPA extrudes  $N_2$  to form the singlet nitrene, **INT**. The singlet nitrene physisorbs more strongly to the graphene surface ( $\Delta E_{ads}$ , G = -18.9 kcal·mol<sup>-1</sup>;  $\Delta E_{ads,G/Cu} = -25.4$  kcal·mol<sup>-1</sup>) than the azide, and the difference in strength between G and G/Cu, 6.5 kcal·mol<sup>-1</sup>, exceeds that with PFPA, likely a consequence from enhanced charge transfer facilitated by the low lying LUMO of the nitrene. The metal substrate serves to substantially stabilize and promote the formation of the nitrene. The physisorbed nitrene then undergoes aziridination to the graphene layer with low energy barriers in each case to form the aziridine final state, **FS**. Since the activation barrier from the nitrene is so low in energy (2.9 kcal·mol<sup>-1</sup> for G and 2.5 kcal·mol<sup>-1</sup> for G/Cu), the relative stabilities of the physisorbed nitrene should help explain the origin of the activation enhancement using a metal substrate.



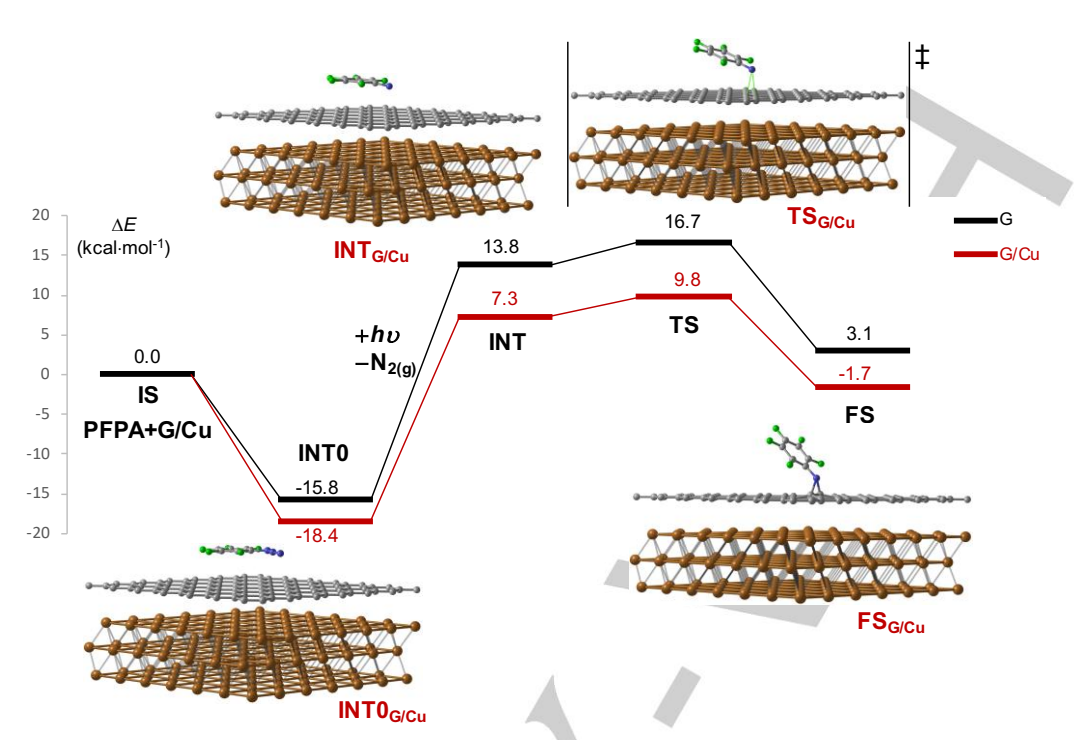


Figure 4. Reaction energy profiles for the aziridination using free-standing graphene (black) and G/Cu (red). Molecular representations for the G/Cu pathway are shown. G=graphene; Cu=Cu(111); G/Cu=graphene supported on Cu; IS=initial state; INT0=PFPA physisorbed on graphene; INT=singlet nitrene intermediate; TS=transition state; FS=aziridine final state.

A reaction pathway including a Ni(111) substrate (G/Ni) was also explored. The corresponding transition state was not located, but the remaining relevant stationary points were located and are compared to those of G and G/Cu (Figure 5). Since Ni is paramagnetic and the ground state of the nitrene is a triplet, the INT<sub>G/Ni</sub> singlet nitrene was obtained using spin-polarized DFT through geometry relaxation with constrained magnetization of the G/Ni unit to that calculated for the isolated G/Ni system until the total magnetization of the nitrene approached zero. The PFPA, INTO, physisorbs more strongly to the G/Ni as compared with the G and G/Cu systems, by 3.4 kcal·mol<sup>-1</sup>. However, the variation in adsorption strength is much greater in the nitrene, INT. The G/Ni substantially stabilizes the nitrene relative to both G (19.2 kcal·mol<sup>-1</sup>) and G/Cu (12.7 kcal·mol<sup>-1</sup>). The relative stabilization of the nitrene between G, G/Cu, and G/Ni coincides with the experimentally observed activation trends and the origin of this enhancement will be explored below.

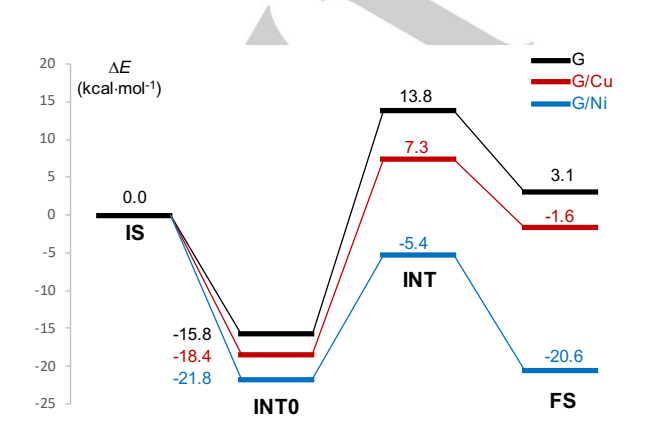
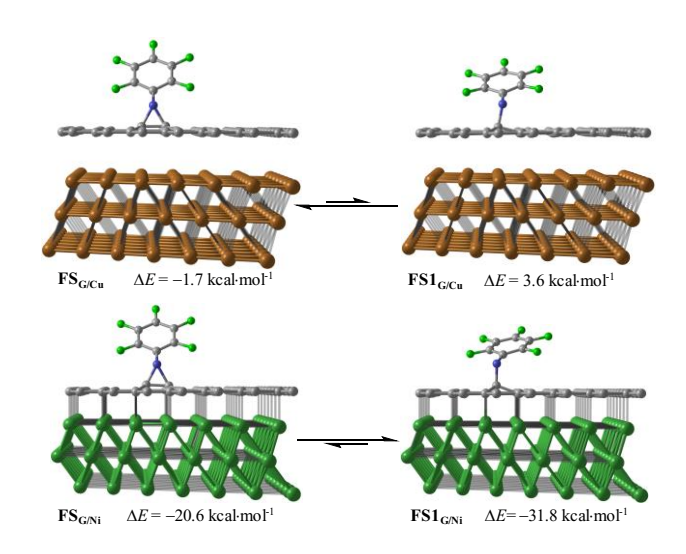


Figure 5. Reaction energy profiles for the aziridination using free-standing graphene (black), G/Cu (red), and G/Ni (blue).

Perhaps unexpectedly, the aziridine is not predicted to be the most stable form of the product for the G/Ni system (Figure 6). An alternative form of the final product may indeed be the open form, **FS1**, rather than the closed aziridine form **FS**. Under the G/Cu system, the open form is less stable by 3.2 kcal·mol<sup>-1</sup>. The open form is not a stable structure in the G system. In contrast, the open product form for the G/Ni system is 10.7 kcal·mol<sup>-1</sup> more stable than the aziridine. The form of the product is therefore predicted to be substrate dependent.



**Figure 6.** Molecular representations and relative energies of the aziridine (**FS**) and open form (**FS1**) final states for G/Cu (top) and G/Ni (bottom). Energies are relative to the initial state, **IS** (Figures. 4 and 5).

The origin of the stability variation in the singlet nitrene was explored through a charge analysis (Figure 7). Charge density on difference surfaces of the adsorbed singlet nitrene were constructed according to the following equation,

$$\Delta \rho(\mathbf{r}) = \rho_{G/M/nitrene}(\mathbf{r}) - (\rho_{G/M}(\mathbf{r}) + \rho_{nitrene}(\mathbf{r}))$$

where  $\rho_{G/M/nitrene}(r)$ ,  $\rho_{G/M}(r)$ , and  $\rho_{nitrene}(r)$  are the electron densities of the graphene/metal/nitrene system, graphene/metal system, and free nitrene respectively. The results reveal regions where charge is both accumulated and depleted upon association of the nitrene. Charge density is being transferred from the graphene surface to the nitrene which is delocalized partially into the aromatic ring, INT<sub>G</sub>. It is clear through visual inspection that a greater amount of charge is transferred to the nitrene in the INT<sub>G/Cu</sub> system. There is little to no change in charge on the Cu(111) cluster as only the charge accumulated on the graphene in the G/Cu system is transferred to the nitrene; no additional charge is transferred from Cu to G to accommodate the loss to the nitrene. Even greater charge is transferred in the INTG/Ni system, but there is also some small amount of back donation of charge from the graphene to the Ni(111). The overall amount of charge transferred,  $\Delta q$ , is quantified through a Bader charge analysis in the same manner in which the charge density surfaces were constructed. Substantially greater charge is transferred from the graphene to the nitrene in the G/Cu system compared to just free-standing graphene, G (cf.  $\Delta q_G = -0.31e$  and  $\Delta q_{G/Cu} = -0.44e$ ). The charge transferred in the G/Ni system is greater than in the G/Cu system ( $\Delta q_{G/Ni}$  = -0.56e). The greater stability in the adsorbed nitrene can in large part be explained by greater charge transfer to the electron deficient nitrene, assisted by its low lying LUMO, from the graphene layer which possesses accumulated charge from the metal substrate. Ni(111) provides the greatest amount of charge on the graphene surface due to greater orbital communication (d  $\rightarrow$  p<sub>z</sub>), as a consequence of greater lattice matching in the top-fcc adsorption pattern with G/Ni.<sup>[15a,40]</sup>

Furthermore, the metal substrates can be shown to lower the nitrene singlet-triplet (ST) energy gap (ΔE<sub>ST</sub>) by stabilizing the singlet relative to the triplet state. Using our method, the calculated ST gap for the isolated 4-methoxycarbonyl-2,3,5,6tetrafluorophenyl nitrene is predicted to be 17.1 kcal×mol<sup>-1</sup>, which is within the range of computed ST gaps for a variety of substituted phenylnitrenes of 16-20 kcal×mol<sup>-1</sup> at the CASPT2 level, [41] providing some validation of our method for predicting ST gaps. The ST gap of the nitrene on free-standing graphene is predicted to be 13.2 kcal×mol<sup>-1</sup>, approximately 4 kcal×mol<sup>-1</sup> lower than the isolated nitrene, demonstrating some degree of singlet stabilization by graphene. With the C/Cu system, the ST gap is further lowered,  $\Delta E_{ST} = 11.5 \text{ kcal·mol}^{-1}$ . The charge being transferred is donated to the empty p orbital of the nitrene nitrogen whereas no such empty orbital of the triplet nitrene can readily accept charge accounting the difference in stabilization. The G/Ni system lowers the ST gap even more to only 6.5 kcal·mol-1. This predicted singlet stabilization relative to the triplet may prevent degradation of the singlet nitrene through intersystem crossing, thus leading to greater activity towards aziridination.

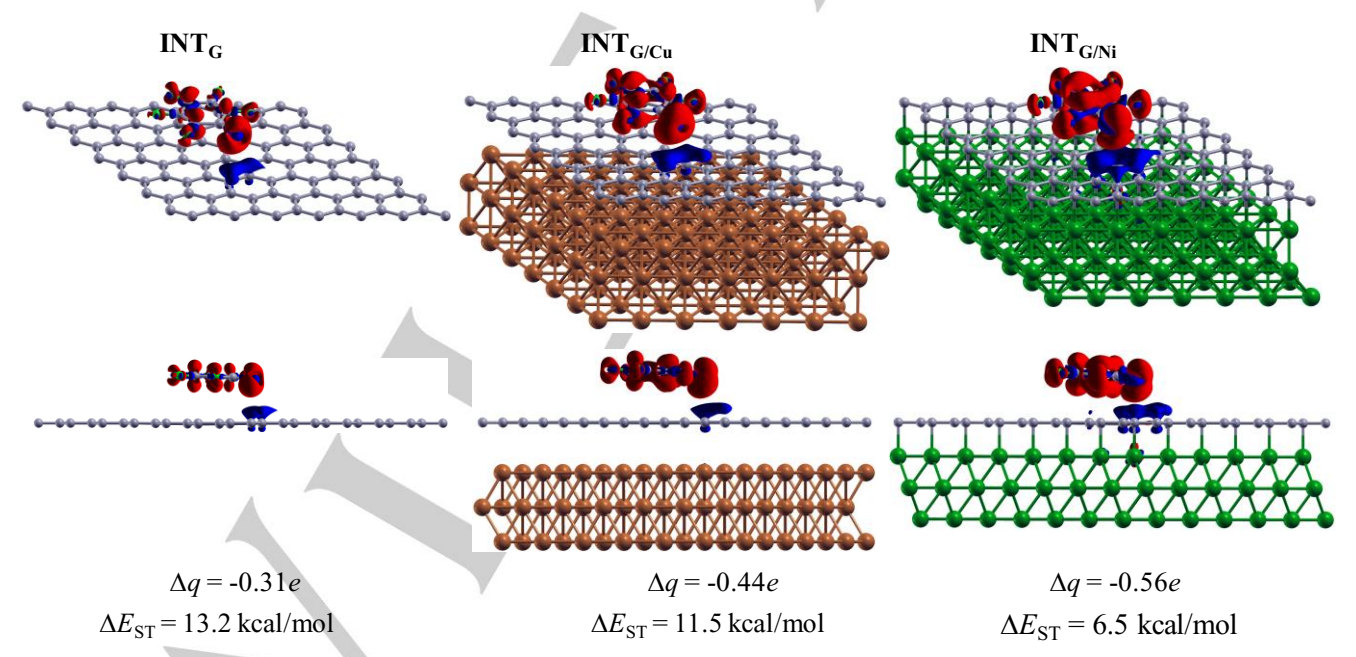


Figure 7. Charge density difference plots of INT<sub>G</sub>, INT<sub>G/Cu</sub>, and INT<sub>G/Ni</sub>. Charge transfers (Δq) are determined from a Bader charge analysis of the electron densities. ΔEST=singlet–triplet (ST) energy gap; Red=charge accumulation; Blue=charge depletion. Isovalue=0.001 e-/bohr3 for each surface.

The computational results suggest that the experimentally observed product rate enhancement may be related to the increased strength of nitrene adsorption to G/Ni or G/Cu relative to G. The substrate influences nitrene formation and stability which may reduce any propensity for accessing unproductive

pathways, thus increasing the rate of desired product formation. The stronger binding using metal substrates is explained by greater charge transfer from the graphene to the nitrene, assisted by the electron rich metals. Intersystem crossing from the singlet to the triplet nitrene is also predicted to be suppressed using metal

#### **FULL PAPER**

substrates by lowering the singlet-triplet gap relative to freestanding graphene when physisorbed to the graphene surface. While this conclusion of singlet-triplet gap lowering by a substrate supported graphene surface is based on theoretical predictions at this stage, the prospect is intriguing and possibly worth verifying experimentally in the future.

#### Conclusion

In summary, we have shown that the reaction of PFPA with graphene was influenced by the substrate on which graphene was supported. Results from Raman spectroscopy and mapping on the extent of functionalization, defect density and reaction kinetics concluded that metal substrate enhances the reactivity of graphene towards PFPA. Computation suggested strong influence of the substrate on the formation and stability of the singlet perfluorophenyl nitrene. The G/Ni substantially stabilizes the singlet nitrene relative to G/Cu and free-standing graphene. The increased stability of the adsorbed nitrene can be attributed to the charge transfer to the electron deficient singlet nitrene from the graphene layer which accumulates charge from the metal substrate, with Ni providing the greatest amount of charge due to the strong orbital communication.

Using the substrate to modulate the chemical reactivity of pristine graphene represents a unique approach in the covalent functionalization of this otherwise inert material. This strategy does not introduce defects to graphene like in the case of holey graphene and can be achieved by a simple transfer procedure from CVD graphene. The findings open up the opportunity to use the substrate as a means to enhance the reactivity of pristine graphene and expand the chemical space of graphene chemistry in general. Equally exciting is the ability to enhance the activity of nitrenes through electron communication with graphene. Arylazides are one of the commonly used photoprobes in photoaffinity labeling, protein ligation and material functionalization, owing to their high stabilities.<sup>[42]</sup> Among the aryl azides, perfluoroaryl azides yield singlet nitrenes having low energy states, extended lifetimes, and high yields in C=C addition and C-H insertion reactions.<sup>[43]</sup> Results from this work demonstrate that the singlet perfluoroaryl nitrenes can be furthermore stabilized by graphene supported on a metal substrate through direct electron communication. This represents a powerful and non-chemical strategy to modulate the reactivity of singlet nitrenes.

#### **Acknowledgements**

The authors are grateful for the financial support from the National Science Foundation (CHE-1808671 to M.Y. and L.M.W.). We thank Prof. YoungJo Kim and Zhen Tian at University of New Hampshire for their generous support in Raman imaging.

Keywords: DFT • graphene • nitrenes • Ni • perfluoroaryl azides

a) S. Du, I. Skachko, A. Barker, E. Y. Andrei, *Nat. Nanotechnol.* **2008**, *3*, 491; b) R. R. Nair, P. Blake, A. N. Grigorenko, K. S. [1] Novoselov, T. J. Booth, T. Stauber, N. M. R. Peres, A. K. Geim, *Science* **2008**, *320*, 1308-1308; c) A. A. Balandin, S. Ghosh, W. Z. Bao, I. Calizo, D. Teweldebrhan, F. Miao, C. N. Lau, *Nano Lett.* **2008**, 8, 902-907; d) J. N. Hu, X. L. Ruan, Y. P. Chen, Nano Lett. 2009, 9, 2730-2735

- D. Li, M. B. Müller, S. Gilje, R. B. Kaner, G. G. Wallace, Nature [2] Nanotechnol. 2008, 3, 101-105.
- [3] a) V. Georgakilas, M. Otyepka, A. B. Bourlinos, V. Chandra, N. Kim, K. C. Kemp, P. Hobza, R. Zboril, K. S. Kim, Chem. Rev. 2012, 112, 6156-6214; b) T. Kuila, S. Bose, A. K. Mishra, P. Khanra, N. H. Kim, J. H. Lee, *Prog. Mater. Sci.* **2012**, *57*, 1061-1105; c) Z. Du, C. Wang, R. Zhang, X. Wang, X. Li, Int. J. Nanomed. 2020, 15, 7523-7551. J. Park, M. Yan, Acc. Chem. Res. 2013, 46, 181-189.
- a) J. Bai, X. Zhong, S. Jiang, Y. Huang, X. Duan, Nat. Nano 2010, 5, 190-194; b) Y. Lin, Y. Liao, Z. Chen, J. W. Connell, Mater. Res. Lett. 2017, 5, 209-234; c) K. Chi, Z. Chen, F. Xiao, W. Guo, W. Xi, J. Liu, H. Yan, Z. Zhang, J. Xiao, J. Liu, J. Luo, S. Wang, K. P. Loh, J. Mater. Chem. A **2019**, 7, 15575-15579; d) W. Xia, J. Tang, J. Li, S. Zhang, K. C. W. Wu, J. He, Y. Yamauchi, *Angew. Chem. Int. Ed.* **2019**, *58*, 13354-13359; *Angew. Chem.* **2019**, *131*, 13488-13493.
- Q. Wu, Y. Wu, Y. Hao, J. Geng, M. Charlton, S. Chen, Y. Ren, H. Ji, H. Li, D. W. Boukhvalov, R. D. Piner, C. W. Bielawski, R. S. Ruoff, [6] Chem. Commun. 2013, 49, 677-679.
- Q. H. Wang, Z. Jin, K. K. Kim, A. J. Hilmer, G. L. C. Paulus, C.-J. [7] Shih, M.-H. Ham, J. D. Sanchez-Yamagishi, K. Watanabe, T. Taniguchi, J. Kong, P. Jarillo-Herrero, M. S. Strano, *Nat. Chem.* **2012**, *4*, 724-732.
- L.-H. Liu, M. Yan, Nano Lett. 2009, 9, 3375-3378.
- [8] [9] a) L.-H. Liu, M. Yan, Acc. Chem. Res. 2010, 43, 1434-1443; b) L.-H. Liu, M. Yan, J. Mater. Chem. 2011, 21, 3273-3276.
- L.-H. Liu, M. M. Lerner, M. Yan, Nano Lett. 2010, 10, 3754-3756. a) L.-H. Liu, G. Zorn, D. G. Castner, R. Solanki, M. M. Lerner, M.
- Yan, J. Mater. Chem. 2010, 20, 5041-5046; b) L.-H. Liu, G. Nandamuri, R. Solanki, M. Yan, J. Nanosci. Nanotechnol. 2011, 11, 1288-1292
- a) J. Park, H. S. Jayawardena, X. Chen, K. W. Jayawardana, M. Sundhoro, E. Ada, M. Yan, *Chem. Commun.* **2015**, *51*, 2882-2885; [12] b) J. Park, T. Jin, C. Liu, G. Li, M. Yan, ACS Omega 2016, 1, 351-
- [13] a) E. Voloshina, Y. Dedkov, Phys. Chem. Chem. Phys. 2012, 14, 13502-13514; b) M. Batzill, Surf. Sci. Rep. 2012, 67, 83-115; c) A. Dahal, M. Batzill, Nanoscale 2014, 6, 2548-2562; d) G. Zhao, X. Li, M. Huang, Z. Zhen, Y. Zhong, Q. Chen, X. Zhao, Y. He, R. Hu, T. Yang, R. Zhang, C. Li, J. Kong, J. B. Xu, R. S. Ruoff, H. Zhu, *Chem. Soc. Rev.* **2017**, *46*, 4417-4449.
- [14] P. A. Khomyakov, G. Giovannetti, P. C. Rusu, G. Brocks, J. van den Brink, P. J. Kelly, Phys. Rev. B: Condens. Matter Mater. Phys. 2009, 79. 195425-195437
- a) Y. Gamo, A. Nagashima, M. Wakabayashi, M. Terai, C. Oshima, *Surf. Sci.* **1997**, 374, 61-64; b) A. Dahal, M. Batzill, *Nanoscale* **2014**, [15] 6, 2548-2562; c) D. E. Parreiras, E. A. Soares, G. J. P. Abreu, T. E. P. Bueno, W. P. Fernandes, V. E. de Carvalho, S. S. Carara, H. Chacham, R. Paniago, *Phys. Rev. B* **2014**, 90, 155454.
- a) W.-B. Zhang, C. Chen, P.-Y. Tang, J. Chem. Phys. 2014, 141, 044708; b) P. L. Silvestrelli, A. Ambrosetti, Phys. Rev. B 2015, 91, 195405
- [17] a) M. Smerieri, E. Celasco, G. Carraro, A. Lusuan, J. Pal, G. Bracco, M. Rocca, L. Savio, L. Vattuone, ChemCatChem 2015, 7, 2328-2331; b) A. Ambrosetti, P. L. Silvestrelli, J. Chem. Phys. 2016, 144, 111101-111105; c) E. Celasco, G. Carraro, M. Smerieri, L. Savio, M. Rocca, L. Vattuone, J. Chem. Phys. 2017, 146, 104704; d) L. Zhu, W. Zhang, J. Zhu, D. Cheng, Carbon 2017, 116, 201-209; e) X. Lin, J. Ni, C. Fang, J. Appl. Phys. 2013, 113, 034306.
- [18] X. Yang, M. Yan, Nano Res. 2020, 13, 599-610.
- [19] Y. Y. Wang, Z. H. Ni, Z. X. Shen, H. M. Wang, Y. H. Wu, Appl. Phys. Lett. 2008, 92, 043121.
- a) A. Allard, L. Wirtz, Nano Lett. **2010**, 10, 4335-4340; b) D. Y. [20] Usachov, V. Y. Davydov, V. S. Levitskii, V. O. Shevelev, D. Marchenko, B. V. Senkovskiy, O. Y. Vilkov, A. G. Rybkin, L. V. Yashina, E. V. Chulkov, I. Y. Sklyadneva, R. Heid, K. P. Bohnen, C. Laubschat, D. V. Vyalikh, ACS Nano 2017, 11, 6336-6345.
- [21] S. D. Costa, A. Righi, C. Fantini, Y. Hao, C. Magnuson, L. Colombo, R. S. Ruoff, M. A. Pimenta, Solid State Commun. 2012, 152, 1317-1320
- [22] E. H. Martins Ferreira, M. V. O. Moutinho, F. Stavale, M. M. Lucchese, R. B. Capaz, C. A. Achete, A. Jorio, Phys. Rev. B 2010,
- [23] K. S. Kim, Y. Zhao, H. Jang, S. Y. Lee, J. M. Kim, K. S. Kim, J. H. Ahn, P. Kim, J. Y. Choi, B. H. Hong, Nature 2009, 457, 706-710.
- L. G. Cancado, A. Jorio, E. H. Ferreira, F. Stavale, C. A. Achete, R. [24] B. Capaz, M. V. Moutinho, A. Lombardo, T. S. Kulmala, A. C. Ferrari, Nano Lett. 2011, 11, 3190-3196.
- [25] a) A. C. Ferrari, D. M. Basko, Nat. Nanotechn. 2013, 8, 235; b) J. Lee, S. Shim, B. Kim, H. S. Shin, Chem. 2011, 17, 2381-2387.
  - a) T. Kubo, X. Wang, Q. Tong, M. Yan, Langmuir 2011, 27, 9372-9378; b) G. Zorn, L.-H. Liu, L. Arnadottir, H. Wang, L. J. Gamble, D. G. Castner, M. Yan, J. Phys. Chem. C 2014, 118, 376-383; c) G. Zorn, D. G. Castner, A. Tyagi, X. Wang, H. Wang, M. Yan, *J. Vac. Sci. Technol., A* **2015**, *33*, 021407; d) N. Kong, J. Park, X. Yang, O. Ramstroem, M. Yan, ACS Appl. Bio Mater. 2019, 2, 284-291.

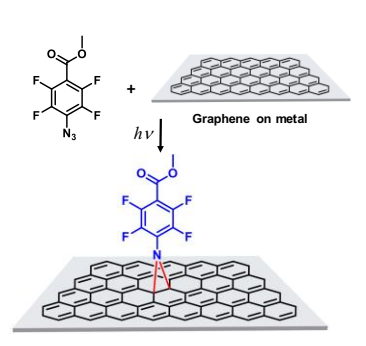
### **FULL PAPER**

- [27] C. O. Ania, B. Cabal, C. Pevida, A. Arenillas, J. B. Parra, F. Rubiera, J. J. Pis, Water Res. 2007, 41, 333-340.
- [28] [29] T. S. Sreeprasad, V. Berry, Small 2013, 9, 341-350.
- Zhao, S. P. Surwade, Z. Li, H. Liu, Nanotechnol. 2012, 23, 355703
- [30]
- R. J. Nemanich, S. A. Solin, *Phys. Rev. B* 1979, *20*, 392-401.
  aZ. Ni, Y. Wang, T. Yu, Z. Shen, *Nano Res.* 2008, *1*, 273-291; bA.
  Das, S. Pisana, B. Chakraborty, S. Piscanec, S. K. Saha, U. V.
  Waghmare, K. S. Novoselov, H. R. Krishnamurthy, A. K. Geim, A. [31] C. Ferrari, A. K. Sood, Nat. Nanotechnol. 2008, 3, 210.
- [32] L. G. Cançado, A. Jorio, E. H. M. Ferreira, F. Stavale, C. A. Achete, R. B. Capaz, M. V. O. Moutinho, A. Lombardo, T. S. Kulmala, A. C. Ferrari, Nano Lett. 2011, 11, 3190-3196.
- [33] M. M. Lucchese, F. Stavale, E. H. M. Ferreira, C. Vilani, M. V. O. Moutinho, R. B. Capaz, C. A. Achete, A. Jorio, Carbon 2010, 48, 1592-1597
- [34] J. M. Englert, P. Vecera, K. C. Knirsch, R. A. Schäfer, F. Hauke, A. Hirsch, ACS Nano 2013, 7, 5472-5482.
- X. Zhang, D. Luo, H. Zhang, D. Y. Hwang, S. O. Park, B.-W. Li, M. Biswal, Y. Jiang, Y. Huang, S. K. Kwak, C. W. Bielawski, R. S. Ruoff, [35] Chem. Mater. 2019, 31, 8639-8648.
- J. Li, M. Li, L. L. Zhou, S. Y. Lang, H. Y. Lu, D. Wang, C. F. Chen,
  L. J. Wan, J. Am. Chem. Soc. 2016, 138, 7448-7451.
  a) B. Hammer, L. B. Hansen, J. K. Nørskov, Phys. Rev. B 1999, 59, [36]
- [37] 7413-7421; b) M. Ernzerhof, G. E. Scuseria, J. Chem. Phys. 1999, 110, 5029-5036; c) J. P. Perdew, K. Burke, M. Ernzerhof, Phys. Rev. Lett. 1996, 77, 3865-3868.
- a) S. Grimme, *J. Comput. Chem.* **2006**, *27*, 1787-1799; b) V. Barone, M. Casarin, D. Forrer, M. Pavone, M. Sambi, A. Vittadini, *J. Comput.* [38] Chem. 2009, 30, 934-939.
- G. Giovannetti, P. A. Khomyakov, G. Brocks, V. M. Karpan, J. van den Brink, P. J. Kelly, *Phys. Rev. Lett.* **2008**, *101*, 026803. [39]
- a) M. Fuentes-Cabrera, M. I. Baskes, A. V. Melechko, M. L. Simpson, [40] Phys. Rev. B 2008, 77, 035405; b) S.-G. Wang, X.-Y. Liao, D.-B. Cao, Y.-W. Li, J. Wang, H. Jiao, J. Phys. Chem. C 2007, 111, 10894-10903
- W. T. G. Johnson, M. B. Sullivan, C. J. Cramer, *Int. J. Quantum Chem.* **2001**, *85*, 492-508. [41]
- [42] a) J. V. Staros, Trends Biochem. Sci. 1980, 5, 320-322; b) N. Gritsan, M. Platz, *Photochemistry of Azides: The AzideNitrene Interfaces*, John Wiley & Sons Ltd., **2010**, pp. 311-372; c) S. J. Lord, H.-I. D. Lee, R. Samuel, R. Weber, N. Liu, N. R. Conley, M. A. Thompson, R. J. Twieg, W. E. Moerner, *J. Phys. Chem. B* **2010**, *114*, 14157-14167; d) E. Leyva, M. S. Platz, S. E. Loredo-Carrillo, J. Aguilar, *Curr. Org. Chem.* **2020**, *24*, 1161-1180; e) X. Kang, X. Cai, L. Yi, Z. V. S., A. H. Winter, C. M. Hadad, *Chapter 2: Theory and*
- [43] Computation in the Study of Nitrenes and Nitrenium Ions, John Wiley & Sons, Inc., Hoboken, 2013, pp. 33-76.



## **FULL PAPER**

#### **Entry for the Table of Contents**



The covalent functionalization of pristine graphene activated by metal substrates towards nitrenes is presented. Observed rate constants reveal that graphene supported on Ni (G/Ni) has the highest reactivity towards nitrenes, followed by G/Cu and then G/silicon wafer. DFT results indicate that increased charge transfer to graphene contribute to the higher reactivity with G/Ni. These results suggest that substrate activation represents an effective and novel strategy for functionalizing graphene using nitrenes potentially extending to other electron deficient reactants.

